Winding Thermal Modeling and Parameters Identification for Multi-Three Phase Machines Based on Short-Time Transient Tests

Winding Thermal Modeling and Parameters Identification for Multi-Three Phase Machines Based on Short-Time Transient Tests

Paolo Pescetto, Simone Ferrari, Gianmario Pellegrino, Enrico Carpaneto, and Aldo Boglietti
Dipartimento Energia Galileo Ferraris, Politecnico di Torino, Turin, Italy
paolo.pescetto@polito.it

***Abstract*—Short-time thermal transient identification method was successfully adopted to evaluate the winding thermal parameters of induction motors for industry applications. In this work, the modeling approach and the identification methodology are extended to the more sophisticated case of multiple three-phase machines. The generalized model takes into consideration the mutual heat exchange between the windings as well as the possible causes of temperature mismatch. A complete procedure to evaluate the parameters of the modified model is provided, supported by experimental validation on a 7.5 kW machine with two three-phase windings in contact at slot level. The method covers any type of multiple three-phase machines, whatever the thermal promiscuity of the winding sets: from deep coupling as the ones presented, to the case where only the end-turns are in contact, to the completely decoupled case. The proposed technique can be useful for the machine design and for real-time temperature monitoring during operation.**

***Index Terms*—Thermal Model Identification; Lumped Parameters; Short-Time Transient; Multiple Winding Machines, Multiphase machines.**

NOMENCLATURE

The symbols and notations adopted in the paper are summarized here.

Short time thermal transient for 3-phase motors

R_0	phase resistance at temperature T_0
R_T	phase resistance at temperature T
P_j	DC Joule loss
C_{eq}	winding copper and insulation thermal capacitance
R_{eq}	thermal resistance between winding and stator core
ΔT_∞	theoretical steady state overtemperature ($R_{eq} \cdot P_j$)
τ	time constant ($R_{eq} \cdot C_{eq}$)
W	dissipated thermal energy

Short time thermal transient for DW motors

$R_{1,0}; R_{2,0}$	phase resistances at temperature T_0
$R_{1,T1}; R_{2,T2}$	phase resistances at temperature $T_1; T_2$
$P_{j1}; P_{j2}$	DC Joule losses
$P_{1Fe}; P_{2Fe}$	heat exchange between each coil and iron
P_{12}	heat exchange between the two windings
$C_1; C_2$	thermal capacitances
$R_{1,Fe}; R_{2,Fe}$	thermal resistance between each winding and stator core
R_{12}	thermal resistance between the two windings
$\Delta T_{1,\infty}; \Delta T_{2,\infty}$	theoretical steady state overtemperature
$\tau_1; \tau_2$	time constants ($R_{1,Fe} \cdot C_1$;$R_{2,Fe} \cdot C_2$)
$W_1; W_2$	dissipated thermal energies

I. INTRODUCTION

In the past, the electrical machines design was mainly based on their electromagnetic performance requirements, but recently, the thermal performance has also been taken into account since the machine thermal behavior strongly influences both motor efficiency and reliability [1], [2]. This is the reason why, in the last years, many simulation thermal models have been developed to assist the design of electrical machines [3], [4]. These models are developed according to two main approaches: Lumped Parameters Thermal-Network (LPTN) [5]–[7] or numerical methods [8], [9]. LPTN methods provide faster response with respect to the numerical ones and can be better handled for geometry optimization during the motor design stage [10]–[12].

The extended use of motors with multiple three-phase winding systems in naval and wind applications, and more recently in aviation [13]–[16] has put in evidence the need of accurate thermal models capable of covering the thermal coupling among the different winding sets. The model must be valid for analyzing the thermal behavior in steady state, transient and faulty conditions [17], for properly monitoring the winding conditions and preventing fault occurrence [18] [19].

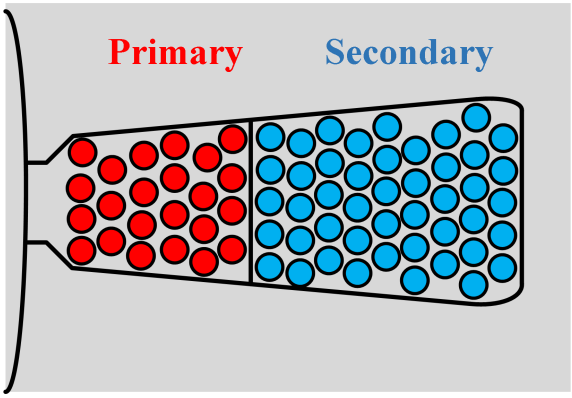

Fig. 1. Schematic of winding allocation in the slot of the DW machine.

This paper deals with a custom designed dual three phase winding machine prototype. The Dual Winding (DW) concept is an innovative technology for starter generators in aerospace application, which is expected to reduce the size of the on-board power electronic converter. Nevertheless, the winding thermal coupling phenomena is a very important issue in DW machines. This technology exploits a Permanent Magnet assisted Synchronous Reluctance (PM-SyR) machine having a stator with two sets of three-phase windings, called primary and secondary. This is a non-conventional case of multiple three-phase machine. The two windings have different number of turns and wire cross section, and so different resistance and leakage inductance. Moreover, the two three-phase sets are fed by different currents from different converters. Every stator slot is occupied by both the sets of windings, one placed in the innermost part of each slot and the other one in the outermost. Therefore, they present different thermal behavior and strong thermal coupling, and a deep investigation of its thermal model is necessary for a full exploitation of the machine.

In this paper, a LPTN able to represent the dynamic thermal behaviors of the two windings and their thermal coupling is presented and deeply analyzed. The procedure for the thermal parameters determination, composed by three tests, is discussed. Two mathematical approaches are proposed for the parameters computation: the first one, approximated but simple, can be used for fast evaluation of the LPTN parameters. The second one is based on an analytical approach. The two methods gave similar results. This extends the applicability of the thermal identification method called "short time thermal transient" to the more complex case of multiple-three phase machines.

The proposed procedure can be usefully adopted for 1) improving the accuracy of the steady-state and transient thermal estimate during the machine design, 2) building a simple and accurate transient thermal model that can be used for online temperature monitoring [20] of highly overloaded machines, or fault tolerant machines when one sector fails or for the prognostics of the windings failure in critical applications.

This paper extends the work in [21] adding a more detailed analysis of the thermal modeling of the machine. Relevant aspects on the parameters estimation, and in particular the mutual heat exchange between the two winding sets, are also highlighted. Moreover, the conference paper relies on a second order lumped parameters thermal model. The possibility to extend the proposed procedure to a third order model, including iron parameters and its temperature variation, is extensively discussed in the new paper. Finally, both the two approaches proposed for the manipulation of the measured data are better described.

II. LPTN of Multiple Three-Phase Machines

The DW machine used for the experimental measurements is a 4 pole/36 slots PM-SyR machine prototype with ferrite permanent magnets. Table I reports its main parameters and characteristics. Each windings set is a standard three-phase single-layer full-pitch winding. The two sets are overlapped and placed in the same slots, as shown in Fig. 1, with a cross-section proportional to the number of turns of each set.

TABLE I
DW machine specifications

	Primary	Secondary
Rated power [kW]	7.5	
Rated speed [rpm]	3000	
Rated load current [A]	40	
DC link voltage [V]	270	
Number of pole pairs	2	
Number of slots	36	
Number of turns in series per phase	30	60
Phase resistance [$m\Omega$]	194	372
Copper Mass [kg]	2.1	4.5

According to the requirements of the DW technology, the number of turns of the secondary winding is higher respect to the primary one, while the two three-phase sets can have different wire section, resulting in different stator resistances. If the two 3-phase sets are connected in series, the DW machine becomes a standard single winding machine.

A. Review of the Three-Phase Case

Previous works [18], [19], [22] demonstrated the effectiveness of the short-time thermal transient method to identify the parameters of a LPTN. The technique was tested in real operating conditions on various three-phase induction motors of different size for industrial application. The adopted model is shown in Fig. 2(a), where the current generator stands for resistive Joule loss P_j in the winding, the capacitor C_{eq} represents the aggregate thermal capacitance of winding plus insulation, the resistor R_{eq} is the thermal resistance from the winding to the stator core iron and T_0 is the initial temperature of the system.

The essential hypotheses behind this method is that during the identification session the stator iron temperature is considered constant and equal to the initial temperature T_0. This hypothesis is supported thanks to the short duration of the identification test. Conversely, if the model presented in Fig. 2(a) is used during motor operation, any losses not due to the stator winding (e.g. iron, PM or mechanical losses) would contribute to define the iron temperature, which will be different from T_0. The LPTN would still be valid, but the generators would force different temperature/thermal power. Therefore, the same LPTN can be applied independently by the type of rotor.

Starting with the motor at room temperature T_0, the three phases are connected in series and excited with direct current while the resistance is online monitored. The amplitude of the injected current is in the order of magnitude of the rated value. Since the initial temperature T_0 and winding resistance R_0 are known, the average winding temperature can be estimated exploiting the well known dependency of the stator resistance with temperature:

$$T = \frac{R_T}{R_0} \cdot (234.5 + T_0) - 234.5 \tag{1}$$

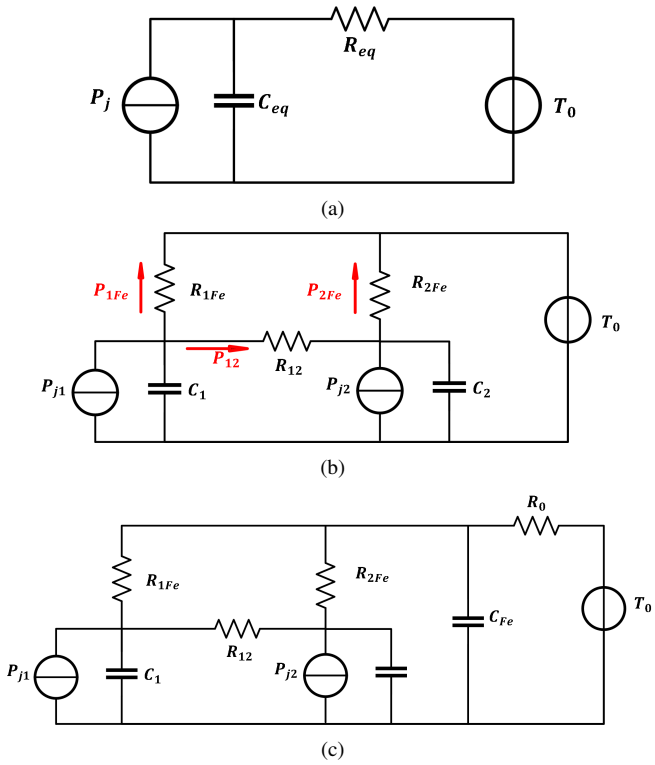

Fig. 2. LPTN for a) single and b) double three-phase winding machines considering constant iron temperature and c) double three-phase winding including finite thermal capacitance of the iron.

where R_T is the winding resistance at the temperature T and 234.5 is the inverse of copper temperature coefficient. In this concern, it must be remarked that the proposed LPTN estimates the average winding temperature. If the LPTN is adopted for assisting the machine design stage, the eventual presence of hot-spots can be taken into account adopting appropriate safety margin or thermal management techniques [23], supported by additional experimental tests. According to the scheme in Fig. 2(a), the thermal transient is approximated by an exponential curve:

$$T(t) = T_0 + \Delta T_\infty \left(1 - e^{-\frac{t}{\tau}}\right) \tag{2}$$

where $\Delta T_\infty = P_j R_{eq}$ and $\tau = R_{eq} C_{eq}$ is the time constant. The initial stage of the temperature transient is approximately adiabatic, i.e. the thermal power P_j directly flows into the equivalent thermal capacitance C_{eq} without affecting the stator iron. As a consequence, no thermal power flows through R_{eq} and the iron core temperature does not change respect to T_0. So, the accumulated energy W versus winding temperature is almost a straight line, whose slope equals the equivalent thermal capacitance:

$$C_{eq} = \frac{dW}{dT} \tag{3}$$

After evaluating C_{eq} from (3), the thermal transient is analytically interpolated with an exponential function based on (2). Then, the equivalent resistance R_{eq} is extracted from the time constant τ of the fitting curve. More details can be found in [18] [19].

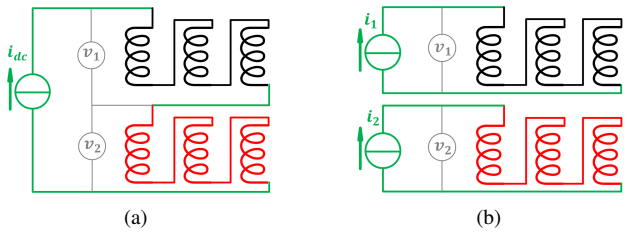

Fig. 3. Winding configuration for a) test "all windings" and b) tests "primary only" and "secondary only".

It should be remarked that the short time thermal transient identification method is essentially experimental based. Therefore, it is able to evaluate the C_{eq} (aggregating the winding copper, insulation and eventual impregnation) and R_{eq} (aggregating any heat transfer from the winding to the stator core) whatever winding material and slot geometry are adopted.

B. Multiple Three-phase Windings

The LPTN of a dual three-phase machine, and namely of the DW machine under test, is reported in Fig. 2(b). Each three-phase set of windings has its proper thermal capacitance, called C_1 and C_2, aggregating the respective winding copper and insulation. Moreover, two thermal power generators P_{j1} and P_{j2} represent the respective stator Joule losses. Each winding exchanges heat with the stator iron through the thermal resistances R_{1Fe} and R_{2Fe}. Moreover, a quota of thermal power P_{12} is exchanged between the two windings, flowing through the resistance R_{12}. It must be remarked that in this specific machine the two windings share the same slots, as can be seen in Fig. 1. Therefore, the contact surface between them is relatively high compared with other types of multiple three-phase machines adopting, for example, different slots for the different winding sets. For this reason, the heath exchange between the two windings is particularly significant, and the value of R_{12} is comparable with R_{1Fe} and R_{2Fe}.

It should be remarked that the LPTN in Fig. 2(b) is a general model including the standard three-phase machines. Indeed, for single three-phase case, the second three-phase set is not present, so the parameters R_{2Fe}, R_{12}, P_{j2} and C_2 vanish and the LPTN is reduced to the one in Fig. 2(a).

In principle, the stator iron has its thermal capacitance, too. The inclusion of finite iron thermal capacitance C_{Fe} leads to the LPTN represented in Fig. 2(c), where R_0 represents the thermal resistance between the iron and the outside air. It must be noted that the temperature variability of the iron along the stator is relevant. Therefore, considering an average iron temperature is commonly a rough approximation. However, thanks to the adiabatic hypothesis, the iron temperature can be considered constant during the first part of the transient (approximately one minute), when the core is not considerably heated. Therefore, the LPTN of Fig. 2(c) will not be used in the following. The scheme of Fig. 2(b) will be used instead, where the iron is represented by the voltage generator T_0. In other words, the thermal capacitance of the iron is initially considered as infinite.

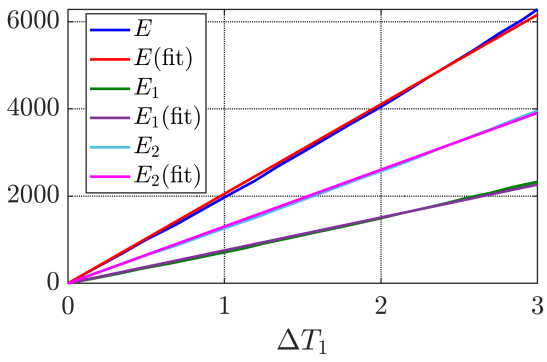

(a)

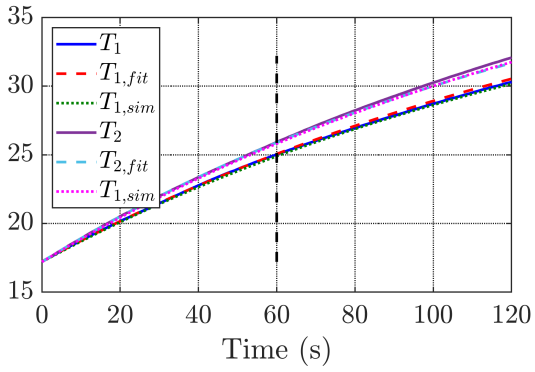

(b)

Fig. 4. (a) Energy Vs overtemperature and (b) temperature transient in the first test (all windings). Solid lines: measured data. Dashed: interpolation based on the first 60 seconds using (8a) and (8b). Dotted: simulation with LPTN in Fig. 2(b).

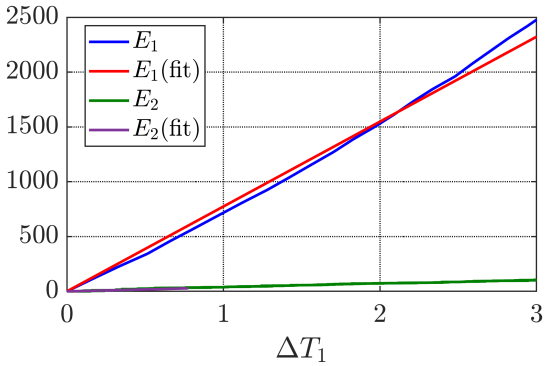

(a)

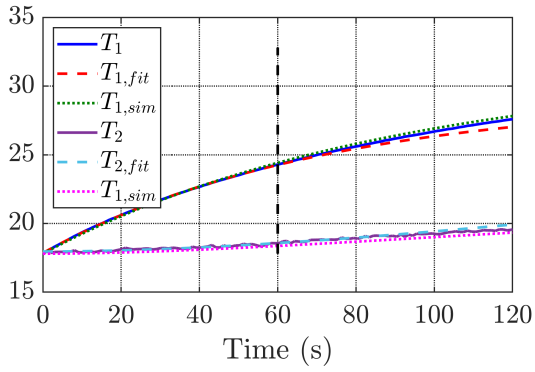

(b)

Fig. 5. (a) Energy Vs overtemperature and (b) temperature transient in the test 2 (primary only). Solid lines: measured. Dashed: interpolation based on the first 60 seconds using (13) and (17). Dotted: simulation with LPTN in Fig. 2(b).

C. Test Sequence

The test procedure described in Section II-A is slightly complicated here to find the five parameters of the LPTN represented in Fig. 2(b). The three phases of each winding set are always series connected, as shown in Fig. 3. The identification procedure consists of three tests:

1) **all windings**: primary three-phase set connected in series to secondary, and excited with constant current $i_{dc} = 20\ A$;
2) **primary only**: the two windings are separated and only the primary channel is excited at 20 A;
3) **secondary only**: the two windings are separated and only the secondary channel is excited at 20 A;

The 20 A excitation current is chosen of the same order of magnitude of the rated current of each winding set. During the test, the DC resistances of the two windings R_1 and R_2 are online measured using the voltage measurement indicated in Fig. 3, divided by the imposed current. The series connection in the test "all windings" guarantees that exactly the same current flows into the two winding sets. In the "primary only" and "secondary only" tests, a small current (1 A) is injected into the non excited winding. This current is only necessary for online monitoring the winding resistance, but it has negligible thermal effect.

Based on the measured resistances, the average temperatures of the two windings are estimated:

$$T_1 = \frac{R_{1,T1}}{R_{1,0}} \cdot (234.5 + T_0) - 234.5 \tag{4a}$$

$$T_2 = \frac{R_{2,T2}}{R_{2,0}} \cdot (234.5 + T_0) - 234.5 \tag{4b}$$

where $R_{1,T1}$ and $R_{2,T2}$ are the two resistances at the temperatures T_1 and T_2 and $R_{1,0}$ and $R_{2,0}$ are the resistances at the initial temperature T_0. The thermal energy dissipated in the two windings is calculated from the electric power:

$$W_1 = \int v_1 \cdot i_1 dt \tag{5a}$$

$$W_2 = \int v_2 \cdot i_2 dt \tag{5b}$$

D. Rapid Data Manipulation: test 1

After measuring the thermal transient, the parameters of the equivalent LPTN are obtained via data manipulation. In the first test ("all windings"), the two windings present similar power loss density and their temperature rises are similar. For this reason, it is assumed that the thermal energy exchange P_{12}

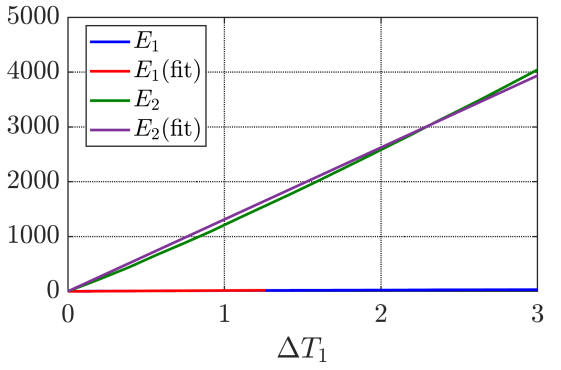

(a)

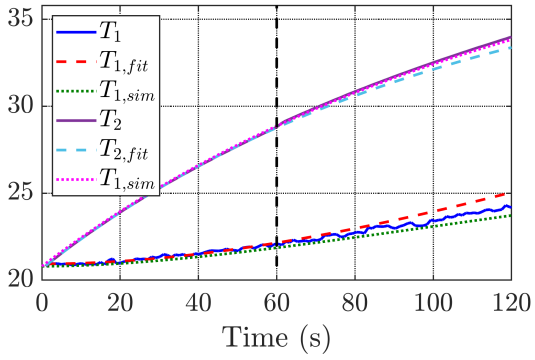

(b)

Fig. 6. (a) Energy Vs overtemperature and (b) temperature transient in the test 3 (secondary only). Solid lines: measured data. Dashed: interpolation based on the first 60 seconds using (13) and (17). Dotted: simulation with LPTN in Fig. 2(b).

between the two windings can be neglected, so the thermal network is simplified as in Fig. 7(a).

$$P_{12} = 0 \tag{6}$$

By using this simplified model, the windings are decoupled and separately studied as two independent single winding machines. Therefore, the same procedure described in Section II-A is adopted to evaluate R_{1Fe}, R_{2Fe}, C_1 and C_2. In particular, the thermal capacitances are obtained from the slope of the dissipated energy as a function of the overtemperature approximated with a straight line, while the resistances are computed from the time constants of the fitting exponential functions:

$$C_1 = \frac{dW_1}{dT_1} \tag{7a}$$

$$C_2 = \frac{dW_2}{dT_2} \tag{7b}$$

$$T_1(t) = T_0 + \Delta T_{1,\infty}\left(1 - e^{-\frac{t}{\tau_1}}\right) \tag{8a}$$

$$T_2(t) = T_0 + \Delta T_{2,\infty}\left(1 - e^{-\frac{t}{\tau_2}}\right) \tag{8b}$$

where $\Delta T_{1,\infty} = P_{j1}R_{1Fe}$ and $\Delta T_{2,\infty} = P_{j2}R_{2Fe}$ are the asymptotic maximum overtemperature and $\tau_1 = R_{1Fe}C_1$ and $\tau_2 = R_{2Fe}C_2$ are the thermal time constants.

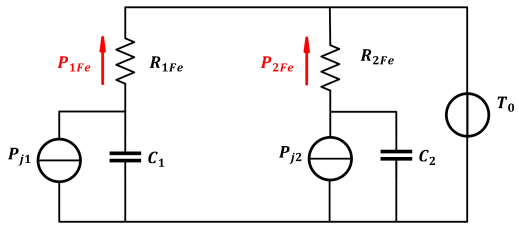

(a)

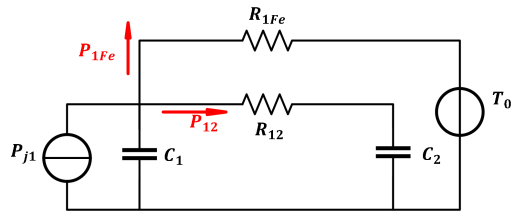

(b)

Fig. 7. LPTN in the test where (a) the winding are series connected and (b) primary winding only is excited.

E. Rapid Data Manipulation: test 2 and 3

In the second test ("primary only"), the temperature of the secondary winding varies by less than 1 °C respect to the initial room temperature. Therefore the heat exchange between the secondary coil and the iron is negligible. Moreover, it is considered that the power loss in the secondary winding is null:

$$P_{2Fe} = 0 \tag{9}$$

$$P_{j2} = 0 \tag{10}$$

The LPTN is then simplified as in Fig. 7(b). It must be remarked once more that this analysis is valid only in the initial part of the thermal transient, when adiabatic condition holds (60 seconds). Using the simplified circuit, the power flow between the two windings is:

$$P_{12} = C_2\frac{dT_2}{dt} \tag{11}$$

where C_2 is retrieved from the first test using (7b). The mutual exchange thermal resistance R_{12} is calculated after the exchanged power P_{12}, as:

$$R_{12} = \frac{T_1 - T_2}{P_{12}} \tag{12}$$

It must be noted that T_1, T_2 and P_{12} are a function of time, therefore a variable R_{12} is found through (12). Anyway, the thermal system is linear, so the value of R_{12} changes very little and it can be reasonably considered as constant. To prove this assert, the time dependency of R_{12} is plotted in Fig. 8. As can be seen, after an initial transient the computed resistance becomes reasonably constant. The average of $R_{12}(t)$ in the first 60 s is reported in Table II.

If numerical optimization wants to be pursued, it can be useful to retrieve an analytical expression of T_1 and T_2. For

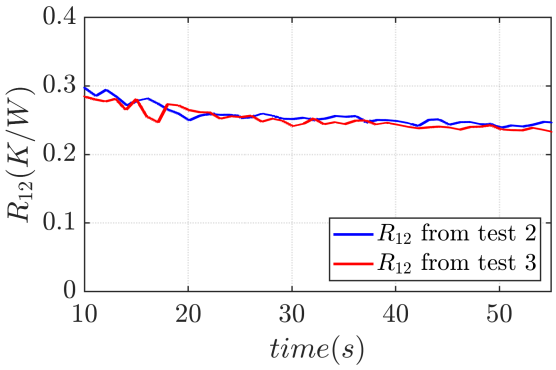

Fig. 8. Variation of R_{12} with time when calculated by (12).

doing so, different hypothesis are separately adopted. According to the LPTN of Fig. 7(b), if the temperature variation of the secondary winding is neglected T_1 follows a first order exponential transient:

$$T_1(t) = T_0 + \Delta T'_{1,\infty}\left(1 - e^{-\frac{t}{\tau'_1}}\right) \tag{13}$$

where $\Delta T'_{1,\infty} = P_{j1}R_{1,eq}$, $\tau'_1 = C_1 R_{1,eq}$ and $R_{1,eq} = R_{12} \parallel R_{1,Fe}$. The advantage of this formulation is that it is suitable for numeric optimization, since P_{j1} is measured and $R_{1,Fe}$ and C_1 are known form the test "all windings".

After calculating T_1 through (13), different hypothesis are adopted to find an analytical expression of T_2. In this case, the primary winding is seen as a current generator providing the thermal power P_{12}. Therefore, the temperature in the secondary winding is approximated as:

$$T_2(t) = T_0 + \frac{1}{C_2}\int_0^t P_{12}\, dt \tag{14}$$

From (12) and (13):

$$T_2(t) = T_0 + \frac{1}{C_2}\int_0^t \frac{T_1 - T_2}{R_{12}}\, dt \tag{15}$$

$$\approx T_0 + \frac{1}{C_2 R_{12}}\int_0^t \Delta T'_{1,\infty}\left(1 - e^{-\frac{t}{\tau_e}}\right)\, dt \tag{16}$$

By solving (16), an analytical approximated expression is obtained for $T_2(t)$:

$$T_2(t) = T_0 + \frac{P_{j1}R_{1,eq}}{C_2 R_{12}}\left(t + \tau'_1 e^{-\frac{t}{\tau'_1}} - \tau'_1\right) \tag{17}$$

As said, T_2 is measured via R_2, using a small current value (1 A). As a consequence, T_2 is noisy, significantly affecting the derivative in (11). Therefore, it may be necessary to preliminary filter the measured temperatures. Alternatively, an analytical expression of T_2 derivative can be conveniently obtained from (17), assuming constant Joule losses P_{j1}:

$$\frac{dT_2}{dt} = \frac{P_{j1}R_{1,eq}}{C_2 R_{12}}\left(1 + e^{-\frac{t}{\tau'_1}}\right) \tag{18}$$

Finally, the "secondary only" test follows the same steps of the former one. Under the dual hypothesis, R_{12} is calculated

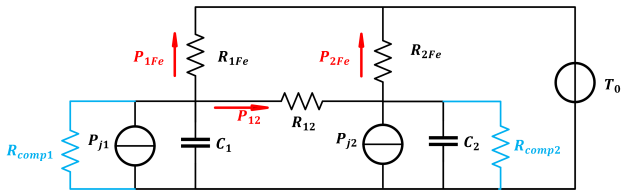

Fig. 9. LPTN adopted for the formal approach data manipulation.

again. Its time dependency is reported in Fig. 8, while its average value among the first 60 s of test is reported in Table II, which reports both the R_{12} estimates obtained from the two tests. The match of R_{12} estimates from the two tests is excellent, proving the consistency of the test sequence. Indeed, the two estimates differ for less than 5 %, which is considered acceptable for most of the LPTN applications.

F. Formal Approach to Data Manipulation

A feasible alternative to the procedure described in Sections II-D and II-E is to analytically solve the LPTN. With constant winding currents, the variation of thermal power due to the dependence of the electrical resistance on the temperature can be modeled with a Norton equivalent circuit, with constant thermal power in parallel to a negative thermal resistance [19]. The negative resistances are required to take into account the increase of dissipated power on varying the winding resistance. Therefore, the LPTN of Fig. 2(b) is modified as in Fig. 9. In this way, the input of the system becomes a step function. Details can be found in [19]. By writing the admittance matrix in Laplace domain, a closed loop solution of the LPTN is analytically retrieved.

Based on the analytical solution it is possible to predict the winding temperature for a given parameters set. The three tests present the same analytical solution, and differ one from the other only for the amplitude of input thermal power. The aggregate Root Mean Square Error ($RMSE$) between measured and predicted temperatures in the three tests is calculated as:

$$RMSE = \sqrt{\frac{\sum_{p=1}^{3}\left(\widehat{T}_1 - T_1\right)^2 + \sum_{p=1}^{3}\left(\widehat{T}_2 - T_2\right)^2}{2\sum_{p=1}^{3}\left(N_p - 1\right)}} \tag{19}$$

where $\widehat{T}_1$ and $\widehat{T}_2$ are the predicted winding temperatures, p is the index of the test and N_p the number of measurement point for a given test. A Nelder-Mead derivative-free optimization algorithm [24] was used to minimize the $RMSE$ calculated in (19), obtaining the parameters set reported in Table II.

As can be noticed, the two proposed methods gave compatible results, and the discrepancy between them is acceptable for the practical application of LPTNs. The advantage of the formal approach is that it permits to easily extended the model to an n^{th} order system, e.g. to take into account finite iron thermal capacitance as in Fig. 2(c). On the other side, it requires more computational effort respect to the rapid data manipulation method.

TABLE II
ESTIMATED PARAMETERS OF THE LPTN.

	C_1 $(J/°C)$	C_2 $(J/°C)$	R_{1Fe} $(°C/W)$	R_{2Fe} $(°C/W)$	R_{12} $(°C/W)$	
Rapid data manipulation	765	1313	0.191	0.131	0.260	0.248
Formal approach	793	1325	0.208	0.146	0.218	

III. EXPERIMENTAL RESULTS

The thermal model identification procedure was experimentally tested on the DW machine described in Section II. The experimental set-up, shown in Fig.c126III, is simple and it only requires two dc current sources, two current and two voltage probes. HBM Gen7i having 18 bit, 0.01% class voltage channels associated to 0.1% class current probes was used.

The three tests described in Section II-C were implemented. Sufficient waiting time ($\approx$ 23 h) was insert between the tests, to ensure that every part of the machine was steadily at ambient temperature before starting the DC excitation. In each test, T_0 was between 20 and 22 °C. For each of the three tests, the resistance variation was online monitored as the ratio between measured voltage and current, and the average temperature was retrieved from (5(b))-(6(b)). The experimentally obtained thermal transients are reported in Figs. 4(b), 5(b) and 6(b).

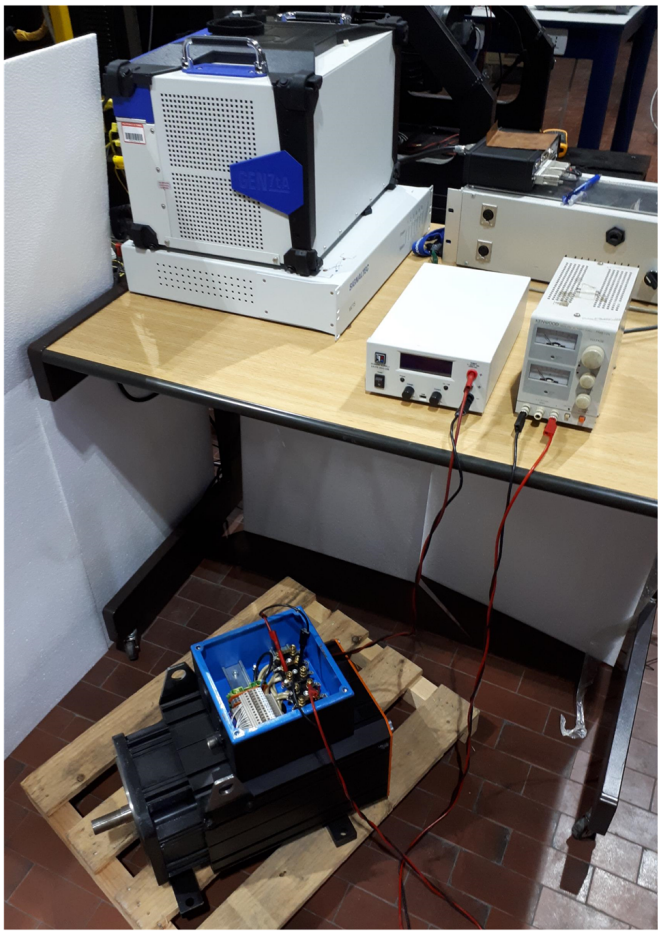

Fig. 10. Experimental setup: dual winding machine, DC power supplies and HBM Gen7i data logger.

It is considered that the hypothesis of short transient operation (e. g. adiabatic conditions) hold up to 60 s. A sufficiently high time range is desirable in order to have a high number of measurement points to be used in the curve fitting and parameters estimation. Conversely, if a too long time limit is chosen the adiabatic conditions fall and the thermal transient can not be well approximated with a first order exponential function. The time window limit was chosen based on the energy Vs overtemperature plot: when adiabatic conditions fall the curve is not anymore represented by a straight line.

Using the obtained parameters, the thermal network of Fig. 2(b) was implemented using Matlab-Simulink. The three tests were simulated imposing the correspondent power loss, and the obtained temperatures were plotted in Fig. 4(b), 5(b) and 6(b) (dotted lines). As can be seen the agreement with the measured temperatures is very good in all the tests. The maximum discrepancy between measured and predicted temperatures up to 120 s is around 1%. For the test "all windings", the discrepancy between the measured and predicted overtemperature in the two windings are bounded between -0.15 and 0.23 °C in the first 180 s of test. In the same time range, the temperature discrepancies for the test "primary only" were limited between -0.28 and 0.32 °C, and for the test "secondary only" between -0.09 and 0.57 °C. In conclusion, the LPTN with the calculated parameters matches very well with the measurement results.

The same Figures also show the temperature transient interpolated with analytical fitting functions based on the first 60 s. The interpolating functions are (8a) and (8b) for the test series, while for the test primary the fitting functions are (13), (17). As can be seen, the complete model of Fig. 2(b) is more accurate, especially after the time frame of 60 s.

IV. FINAL REMARKS

The proposed method aims to identify the LPTN of the stator winding of a dual three-phase machine, which is independent from the rotor type or structure. In other words, despite the DW machine example has a PM-SyR rotor, the proposed procedure applies to other types of synchronous dual three-phase machines and even to induction motors, either with distributed or concentrated windings. This property of the short-time transient thermal identification was demonstrated in [25].

As a further validation of the proposed thermal identification method, the thermal capacitance of the two windings was retrieved based on the estimated amount of copper present in the machine, according to [19]. The two approaches gave similar results. The relative discrepancy was lower than 8 %

V. Conclusion

The characterization of the copper to iron thermal model based on short-time thermal transient identification, already presented for three-phase motors, was successfully extended to multiple three-phase machines. A new lumped parameters thermal model is proposed and validated. This model is valid for an arbitrary number of stator windings and it can be easily applied to any multi-phase machine. Moreover, it can be extended to include finite iron capacitance, increasing the degree of freedom of the thermal network. The test procedure, together with two methods for calculating the parameters of the analytical model where presented and validated on a 7.5 kW dual winding machine prototype. The two post-processing approaches gave compatible results. The proposed model and identification procedure can be usefully adopted for real-time temperature monitoring in critical applications, and as a valid support to the design of multiple three-phase machines.

References

[1] R. Wrobel, P. H. Mellor, M. Popescu and D. A. Staton, "Power Loss Analysis in Thermal Design of Permanent-Magnet Machines—A Review," in *IEEE Transactions on Industry Applications*, vol. 52, no. 2, pp. 1359-1368, March-April 2016.

[2] R. Leuzzi, P. Cagnetta, S. Ferrari, P. Pescetto, G. Pellegrino and F. Cupertino, "Transient Overload Characteristics of PM-Assisted Synchronous Reluctance Machines, Including Sensorless Control Feasibility," in IEEE Transactions on Industry Applications, vol. 55, no. 3, pp. 2637-2648, May-June 2019.

[3] P. H. Mellor, D. Roberts and D. R. Turner, "Lumped parameter thermal model for electrical machines of TEFC design," in *IEE Proceedings B - Electric Power Applications*, vol. 138, no. 5, pp. 205-218, Sept. 1991.

[4] A. Boglietti, A. Cavagnino, D. Staton, M. Shanel, M. Mueller and C. Mejuto, "Evolution and Modern Approaches for Thermal Analysis of Electrical Machines," in *IEEE Transactions on Industrial Electronics*, vol. 56, no. 3, pp. 871-882, March 2009.

[5] A. Boglietti, A. Cavagnino, M. Lazzari and M. Pastorelli, "A simplified thermal model for variable-speed self-cooled industrial induction motor," in *IEEE Transactions on Industry Applications*, vol. 39, no. 4, pp. 945-952, July-Aug. 2003.

[6] N. Rostami, M. R. Feyzi, J. Pyrhonen, A. Parviainen and M. Niemela, "Lumped-Parameter Thermal Model for Axial Flux Permanent Magnet Machines," in IEEE Transactions on Magnetics, vol. 49, no. 3, pp. 1178-1184, March 2013.

[7] P. S. Ghahfarokhi, A. Belahcen, A. Kallaste, T. Vaimann, L. Gerokov and A. Rassolkin, "Thermal Analysis of a SynRM Using a Thermal Network and a Hybrid Model," 2018 XIII International Conference on Electrical Machines (ICEM), Alexandroupoli, 2018, pp. 2682-2688.

[8] W. Jiang, T. M. Jahns, "Coupled Electromagnetic–Thermal Analysis of Electric Machines Including Transient Operation Based on Finite-Element Techniques," in *IEEE Transactions on Industry Applications*, vol. 51, no. 2, pp. 1880-1889, March-April 2015.

[9] I. Bolvashenkov, J. Kammermann, K. Udovichenko, L. Tippe and H. Herzog, "Thermal Steady-State Behavior of 9-Phase Synchronous Machines with Surface Permanent Magnets during Open Phase Faults," 2018 IEEE International Conference on Electrical Systems for Aircraft, Railway, Ship Propulsion and Road Vehicles & International Transportation Electrification Conference (ESARS-ITEC), Nottingham, 2018, pp. 1-6.

[10] C. Kral, A. Haumer and S. B. Lee, "A Practical Thermal Model for the Estimation of Permanent Magnet and Stator Winding Temperatures," in *IEEE Transactions on Power Electronics*, vol. 29, no. 1, pp. 455-464, Jan. 2014.

[11] N. Simpson, R. Wrobel and P. H. Mellor, "Estimation of Equivalent Thermal Parameters of Impregnated Electrical Windings," in *IEEE Transactions on Industry Applications,* vol. 49, no. 6, pp. 2505-2515, Nov.-Dec. 2013.

[12] Y. Bertin, E. Videcoq, S. Thieblin and D. Petit, "Thermal behavior of an electrical motor through a reduced model," in *IEEE Transactions on Energy Conversion,* vol. 15, no. 2, pp. 129-134, Jun 2000.

[13] R. Bojoi, M. G. Neacsu and A. Tenconi, "Analysis and survey of multi-phase power electronic converter topologies for the more electric aircraft applications," *International Symposium on Power Electronics Power Electronics, Electrical Drives, Automation and Motion*, Sorrento, 2012, pp. 440-445

[14] E. Levi, "Multiphase Electric Machines for Variable-Speed Applications," in *IEEE Transactions on Industrial Electronics,* vol. 55, no. 5, pp. 1893-1909, May 2008.

[15] M. Villani, M. Tursini, G. Fabri and L. Castellini, "Multi-phase fault tolerant drives for aircraft applications," *Electrical Systems for Aircraft, Railway and Ship Propulsion*, Bologna, 2010, pp. 1-6.

[16] P. Pescetto, E. Armando and G. Pellegrino, "Commissioning and Sensorless Control of High Power SyR Machine Prototypes," *2019 IEEE 10th International Symposium on Sensorless Control for Electrical Drives (SLED)*, Turin, Italy, 2019, pp. 1-6.

[17] M. Barcaro, L. Alberti and N. Bianchi, "Thermal analysis of dual three-phase machines under faulty operations," 8th IEEE Symposium on Diagnostics for Electrical Machines, Power Electronics & Drives, Bologna, 2011, pp. 165-171.

[18] T. Huber, W. Peters and J. Böcker, "A low-order thermal model for monitoring critical temperatures in permanent magnet synchronous motors," *7th IET International Conference on Power Electronics, Machines and Drives (PEMD 2014)*, Manchester, 2014, pp. 1-6.

[19] A. Boglietti, E. Carpaneto, M. Cossale and S. Vaschetto, "Stator-Winding Thermal Models for Short-Time Thermal Transients: Definition and Validation," in *IEEE Transactions on Industrial Electronics*, vol. 63, no. 5, pp. 2713-2721, May 2016.

[20] N. Jaljal, J. F. Trigeol and P. Lagonotte, "Reduced Thermal Model of an Induction Machine for Real-Time Thermal Monitoring," in IEEE Transactions on Industrial Electronics, vol. 55, no. 10, pp. 3535-3542, Oct. 2008.

[21] P. Pescetto, S. Ferrari, G. Pellegrino, E. Carpaneto and A. Boglietti, "Short-Time Transient Thermal Model Identification of Multiple Three-Phase Machines," *2018 IEEE Energy Conversion Congress and Exposition (ECCE)*, Portland, OR, 2018, pp. 222-228.

[22] A. Boglietti, M. Cossale, S. Vaschetto and T. Dutra, "Winding Thermal Model for Short-Time Transient: Experimental Validation in Operative Conditions," in IEEE Transactions on Industry Applications, vol. 54, no. 2, pp. 1312-1319, March-April 2018.

[23] V. Madonna, A. Walker, P. Giangrande, G. Serra, C. Gerada and M. Galea, "Improved Thermal Management and Analysis for Stator End-Windings of Electrical Machines," in *IEEE Transactions on Industrial Electronics*, vol. 66, no. 7, pp. 5057-5069, July 2019.

[24] Pérez-Arriaga I. J., Verghese G. C., Schweppe F. C., "Selective Modal Analysis with Applications to Electric Power Systems. Part 1: Heuristic Introduction", *IEEE Transactions on Power Apparatus and Systems*, Vol. PAS-101, No. 9, September 1982, pp. 3117-3125

[25] A. Boglietti, M. Cossale, S. Vaschetto and T. Dutra, "Thermal Conductivity Evaluation of Fractional-Slot Concentrated-Winding Machines," in *IEEE Transactions on Industry Applications*, vol. 53, no. 3, pp. 2059-2065, May-June 2017.